

The basic physics of the binary black hole merger GW150914

B. Allen et al. ^a

(LIGO Scientific Collaboration and Virgo Collaboration)

(Dated: June 21, 2016)

Abstract

The first direct gravitational wave detection, GW150914, was strong enough to be seen by eye in the raw detector data. A simple analysis, using only basic physics and features clearly visible in the data, is sufficient to show that the signal was produced by the inspiral and subsequent merger of two black holes. This simple analysis demonstrates that the system was composed of two black holes, each of approximately $35 M_{\odot}$, which last orbited each other at a separation of 350 km and then merged to form a single black hole of approximately $70 M_{\odot}$; no other known type of astrophysical objects could have been responsible for such a signal. Similar considerations are used to roughly estimate the distance. The simple analyses presented here are consistent with the more detailed analyses of the signal, published elsewhere.

^a Full author list given at the end of the article: B. Allen, O. Birnholtz, S. Ghosh, A. Nielsen, A. G. Wiseman
+ LVC 02/2016

I. INTRODUCTION

Advanced LIGO made the first detection of a gravitational wave (GW) signal, GW150914¹, on September 14th, 2015. The signal was clearly seen by the two LIGO detectors located in Hanford, WA and Livingston, LA. Extracting the full information about the source of the signal requires detailed analytical and computational methods (see Refs. 2–4 and references therein for details). However, much can be learned about the source by direct inspection of the detector data and some basic physics. This simple analysis indicates that the source is two black holes (BHs) orbiting around one another and then merging to form another black hole .

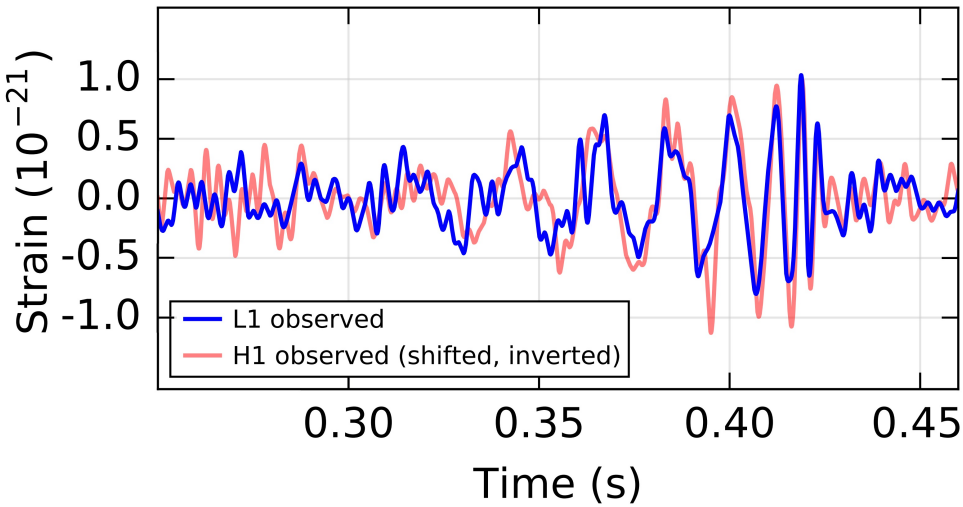


FIG. 1. The instrumental strain data in the Livingston detector (blue) and Hanford detector (red), as shown in Figure 1 of Ref. 1. Both have been filtered. The Hanford strain has been shifted back in time by 6.9 ms and inverted. Times shown are relative to 09:50:45 Coordinated Universal Time (UTC) on September 14, 2015.

A black hole is a region of space-time where the gravitational field is so intense that neither matter nor radiation can escape. There is a natural “gravitational radius” associated with a mass m , called the Schwarzschild radius, given by

$$r_{\text{Schwarz}}(m) = \frac{2Gm}{c^2} = 2.95 \left(\frac{m}{M_\odot} \right) \text{ km}, \quad (1)$$

where $M_\odot = 1.99 \times 10^{30}$ kg is the mass of the Sun. According to the hoop conjecture if a non-spinning mass is compressed to within that radius, then it must form a black hole⁵.

Once the black hole is formed, any object that comes within this radius can no longer escape out of it.

The result that GW150914 was emitted by an inspiral and merger of two black holes follows from (1) the strain data visible at the instrument output, (2) dimensional and scaling arguments, (3) primarily Newtonian orbital dynamics and (4) the Einstein quadrupole formula for the luminosity of a gravitational wave source. These calculations are simple enough that they can be readily verified with pencil and paper in a few minutes. Our presentation is by design approximate, emphasizing simple arguments. Specifically, while the orbital motion of two bodies is approximated by Newtonian dynamics and Kepler's laws to high precision at sufficiently large separations and sufficiently low velocities, we will invoke Newtonian dynamics to describe the motion even at the end point of orbital motion. We revisit this assumption in Sec. IV D. The reader requiring precise numbers describing the system is referred to publications elsewhere^{1–4}.

The paper is organized as follows: our presentation begins with the data output by the detectors⁶. Sec. II describes the properties of the signal read off the strain data, and how they determine the quantities relevant for analyzing the system as a binary inspiral. We then demonstrate in Sec. III, using the most simple assumptions, that the binary constituents must be heavy and small, consistent only with being black holes. In Sec. IV we examine and justify the assumptions made, and constrain both masses to be well above the heaviest known neutron stars. The appendices demonstrate a calculation of gravitational radiation (App. A), and discuss astrophysical compact objects of high mass (App. B) and what one might learn from the waveform's end (App. C).

II. ANALYZING THE OBSERVED DATA

Our starting point is shown in Fig. 1: the instrumentally observed strain data $h(t)$, after applying a band-pass filter to the LIGO sensitive frequency band (35–350 Hz), and a band-reject filter around known instrumental noise frequencies. The time-frequency behavior of the signal is depicted in Fig. 2. An approximate version of the time-frequency evolution can also be obtained directly from the strain data in Fig. 1 by measuring the time difference between successive zero-crossings⁷. Fig. 3 shows the strain data from Fig. 1 overlaid with a waveform template obtained by modeling; it also shows a piecewise-linear fit to the frequencies $f_{\text{GW}}(t)$

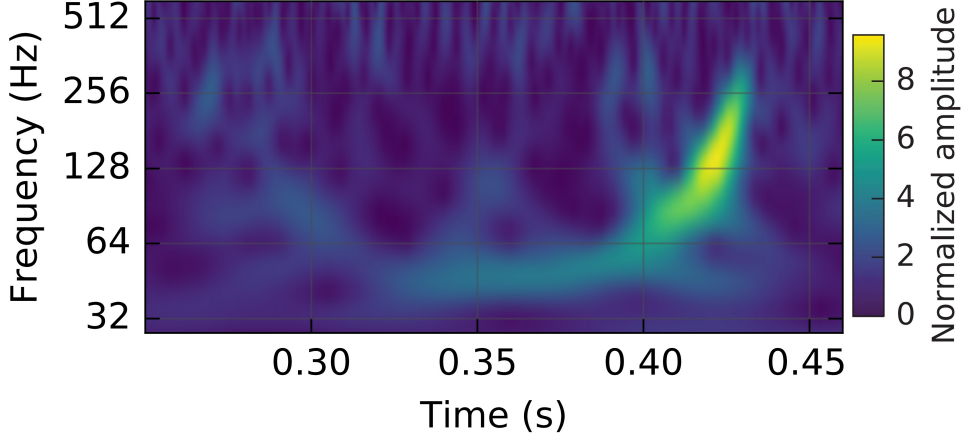


FIG. 2. A representation of the strain-data as a time-frequency plot (taken from Ref. 1), where the increase in signal frequency (“chirp”) can be traced over time.

of the template, interpolated from the zero-crossings. This template is given for convenience, as it can be used – at least during the time-interval where it is a direct visual fit to the strain signal – as an estimate for the signal’s $f_{\text{GW}}(t)$. We stress that the model waveform is being used only as a crutch, to obtain smoothed values for the frequency, frequency-derivative, and amplitude as functions of time. These can also be obtained directly from the data stream, without assuming a waveform model, under the sole assumption that the frequency and amplitude are smoothly-varying functions of time.

The signal is dominated by several cycles of a wave pattern whose amplitude is initially increasing, starting from around the time mark 0.30 s. In this region the gravitational wave period is decreasing, thus the frequency is increasing. After a time around 0.42s, the amplitude drops rapidly, and the frequency appears to stabilize. The last clearly visible cycles (in both detectors, after accounting for a 6.9 ms time-of-flight-delay¹) indicate that the final instantaneous frequency is well above 200 Hz. The entire visible part of the signal lasts for around 0.15 s.

In Einstein’s theory of general relativity (GR), gravitational waves are produced by accelerating masses. Since the waveform clearly shows at least eight oscillations, we know that mass or masses are oscillating. The increase in gravitational wave frequency and amplitude also indicate that during this time the oscillation frequency of the source system is increasing. This initial phase cannot be due to a perturbed system returning back to stable equilibrium, since oscillations around equilibrium are generically characterized by roughly

constant frequencies and decaying amplitudes. For example, in the case of a fluid ball, the oscillations would be damped by viscous forces. Here, the data demonstrate very different behavior.

During the period when the gravitational wave frequency and amplitude are increasing, orbital motion of two bodies is the only plausible explanation. There, the only “damping forces” are provided by gravitational wave emission, which brings the orbiting bodies closer (an “inspiral”), increasing the orbital frequency and amplifying the gravitational wave energy output from the system. Gravitational radiation is at leading order quadrupolar, and the quadrupole moment is invariant under reflection about the center of mass (even for unequal masses). This symmetry implies that the gravitational wave must be radiated at a frequency that is twice the orbital frequency⁸. The eight gravitational wave cycles of increasing frequency therefore require at least four orbital revolutions, at separations large enough (compared to the size of the bodies) that the bodies do not collide. The rising frequency signal eventually terminates, suggesting the end of orbital motion. As the amplitude decreases and the frequency stabilizes the system returns to a stable equilibrium configuration. We shall show that the only reasonable explanation for the observed frequency evolution is that the system consisted of two black holes that had orbited each other and subsequently merged.

Determining the frequency at maximum strain amplitude $f_{\text{GW}}|_{\max}$: The single most important quantity for the reasoning in this paper is the gravitational wave frequency at which the waveform has maximum amplitude. Using the zero-crossings around the peak of Fig. 1 and/or the brightest point of Fig. 2, we take the conservative value

$$f_{\text{GW}}|_{\max} \sim 150 \text{ Hz}. \quad (2)$$

We thus interpret the observational data as indicating that the bodies were orbiting each other (roughly Keplerian dynamics) up to an orbital angular frequency

$$\omega_{\text{Kep}}|_{\max} = 2\pi f_{\text{GW}}|_{\max}/2 = 2\pi \times 75 \text{ Hz}. \quad (3)$$

Determining the mass scale: Einstein found⁹ that the gravitational wave strain h at a distance d_L from a system whose traceless mass quadrupole moment is Q_{ij} (defined in App. A) is

$$h_{ij} = \frac{2G}{c^4 d_L} \frac{d^2 Q_{ij}}{dt^2}, \quad (4)$$

and that the energy carried by these gravitational waves is given by the Quadrupole Formula⁹

$$\frac{dE_{\text{GW}}}{dt} = \frac{c^3}{16\pi G} \iint |\dot{h}|^2 dS = \frac{1}{5} \frac{G}{c^5} \sum_{i,j=1}^3 \frac{d^3 Q_{ij}}{dt^3} \frac{d^3 Q_{ij}}{dt^3}, \quad (5)$$

where the integral is over a sphere at radius d_L (contributing a factor $4\pi d_L^2$), and the quantity on the right-hand side must be averaged over (say) one orbit (see App. A).

In our case, Eq. 5 gives the rate of loss of orbital energy to gravitational waves , when the velocities of the orbiting objects are not too close to the speed of light, and the strain is not too large (we use it until $f_{\text{GW}}|_{\max}$, see Sec. IV D).

For the binary system we denote the two masses by m_1 and m_2 and the total mass by $M = m_1 + m_2$. We define the mass ratio $q = m_1/m_2$ and without loss of generality assume that $m_1 \geq m_2$ so that $q \geq 1$. To describe the gravitational wave emission from a binary system, a useful mass quantity is the *chirp mass*, M_c , related to the component masses by

$$M_c = \frac{(m_1 m_2)^{3/5}}{(m_1 + m_2)^{1/5}}. \quad (6)$$

Using Newton's laws of motion, Newton's universal law of gravitation, and Einstein's quadrupole formula for the gravitational wave luminosity of a system, a simple formula is derived in App. A (following Refs. 10 and 11) relating the frequency and frequency derivative of emitted gravitational waves to the chirp mass,

$$M_c = \frac{c^3}{G} \left(\left(\frac{5}{96} \right)^3 \pi^{-8} (f_{\text{GW}})^{-11} (\dot{f}_{\text{GW}})^3 \right)^{1/5}, \quad (7)$$

where $\dot{f}_{\text{GW}} = df_{\text{GW}}/dt$ is the rate-of-change of the frequency and G is Newton's gravitational constant (see Eq. A4 and Eq. 3 of Ref. 12). This equation is expected to hold as long as the Newtonian approximation is valid (see Sec. IV D).

Thus, the value of the chirp mass can be determined directly from the observational data, by plotting the frequency and frequency derivative of the gravitational waves as a function of time. The value of the chirp mass M_c can be estimated from a time-frequency plot of the observed gravitational wave strain data, using either Fig. 2 or Fig. 3. Over the inspiral period in the band, $30 < f_{\text{GW}} < 150$ Hz. As the frequency (period) varies by a factor of 5 ($\frac{1}{5}$), the frequency derivative varies by a factor of about 25. The chirp mass M_c , however, remains constant to within 25%. The exact value of M_c is not critical to the arguments that we present here, so for simplicity we take $M_c = 30 M_\odot$.

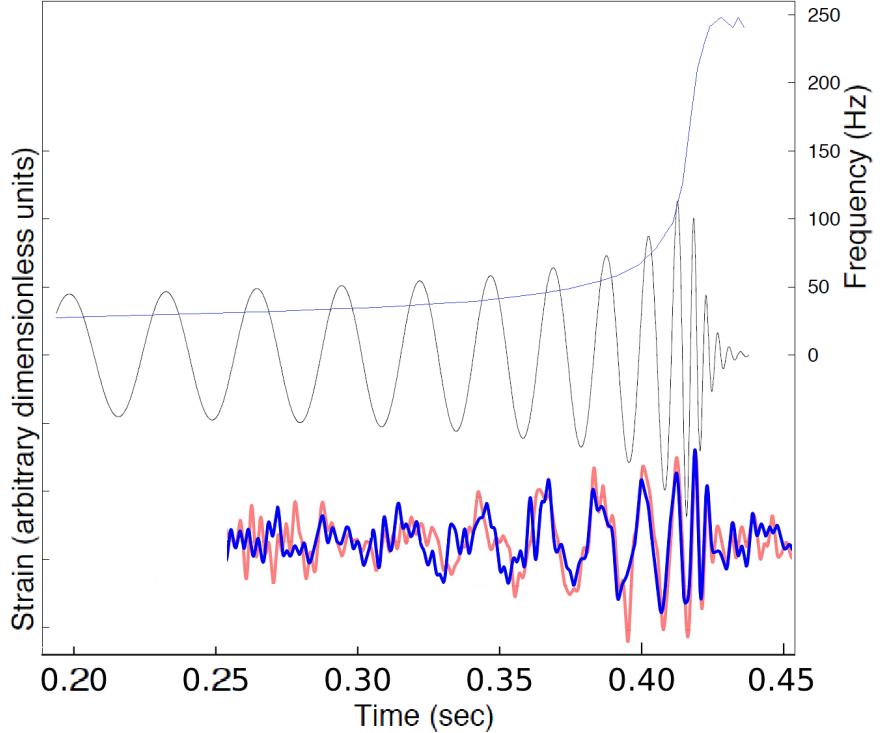


FIG. 3. A best-fit modeled waveform (black, left axis), and the frequency f_{GW} (blue, right axis) of that waveform as a function of time. When $f_{\text{GW}} < 200$ Hz, this is a direct visual match to the observed data, so it gives us a value of gravitational wave frequency as a function of time, $f_{\text{GW}}(t)$. We plot a piecewise-linear function, interpolated between values $f_{\text{GW}} = 1/(2\Delta t)$ where Δt is the time between successive zeros of the strain data.

Note that the characteristic mass scale of the radiating system is obtained by direct inspection of the time/frequency behavior of the observational data (with a the piecewise linear fit).

The fact that the chirp mass remains approximately constant for $f_{\text{GW}} < 150$ Hz is strong support for the orbital interpretation. The fact that the amplitude of the gravitational wave strain increases with frequency also supports this interpretation, and suggests that the assumptions that go into the calculation which leads to these formulas are applicable: the velocities in the binary system are not too close to the speed of light, and the orbital motion has an adiabatically changing radius and period described instantaneously by Kepler's laws. The data also indicate that these assumptions break down at a gravitational wave frequency above $f_{\text{GW}}|_{\max}$, as the amplitude stops growing.

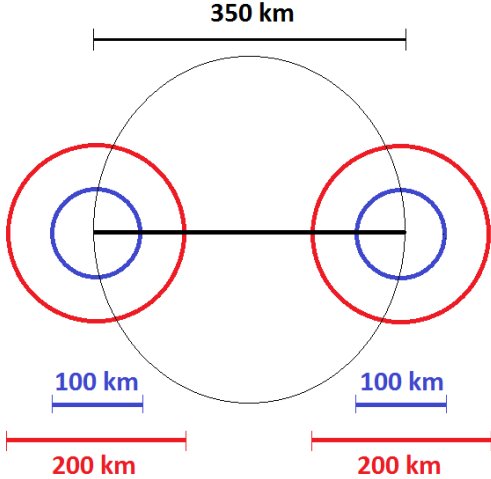


FIG. 4. A demonstration of the compactness of the orbit at minimal separation (black, 350 km) vs. compact radii: Schwarzschild (red, 200 km) and extremal Kerr (blue, 100 km). Note the masses here are equal; as explained in Sec. IV B, the system becomes even more compact for unequal masses.

Alternatively, Eq. 7 can be integrated to the form

$$f_{\text{GW}}^{-8/3}(t) = -\frac{(8\pi)^{8/3}}{5} \left(\frac{G M_c}{c^3} \right)^{5/3} (t - t_0), \quad (8)$$

which does not involve \dot{f}_{GW} , and can therefore be used to calculate M_c directly from the time periods between zero-crossings in the strain data. We have performed such an analysis, to find similar results and we henceforth adopt a conservative lower estimate of $30 M_\odot$. We remark that this mass is derived from quantities measured in the detector frame, thus it and the quantities we derive from it are given in the detector frame. Discussion of redshift from the source frame appears in Sec. IV F.

III. PROVING COMPACTNESS IN THE SIMPLEST CASE

For simplicity, now suppose that the two bodies have equal masses, $m_1 = m_2$. The value of the chirp mass then implies that $m_1 = m_2 = 2^{1/5} M_c = 35 M_\odot$, so that the total mass is $M = m_1 + m_2 = 70 M_\odot$. We also assume for now that the objects are not spinning, and that their orbit remains Keplerian and essentially circular until the point of peak amplitude.

At the time of peak amplitude the bodies therefore had an orbital separation R given by

$$R = \left[\frac{GM}{\omega_{\text{Kep}}^2 |_{\text{max}}} \right]^{1/3} = 350 \text{ km.} \quad (9)$$

Compared to normal orbital length scales for stars, this is a *tiny* value. This constrains the objects to be exceedingly small, or else they would have collided and merged long before reaching such close proximity. Main-sequence stars have radii measured in millions of kilometers, and white dwarf (WD) stars have radii which are typically ten thousand kilometers. Scaling Eq. 9 shows that such stars' inspiral evolution would have terminated at an orbital frequency of a few mHz (far below 1 Hz).

The most compact stars known are neutron stars, which have radii of only about ten kilometers. Two neutron stars could have orbited at this separation without colliding or merging together – but the maximum mass that a neutron star can have before collapsing into a black hole is about $3 M_\odot$ (see App. B).

In our case, the bodies of mass $m_1 = m_2 = 35 M_\odot$ each have a Schwarzschild radius of 103 km. This is illustrated in Fig. 4. If these objects were non-rotating black holes , then the orbital separation of 350 km would have meant that the event horizons of the two black holes were separated¹³ by only about 150 km.

In order to quantify the closeness of the two objects relative to their natural gravitational radius, we introduce the compactness ratio \mathcal{R} . This is defined as the Newtonian orbital separation between the centers of the objects divided by the sum of their smallest possible respective radii (as compact objects). For the non-spinning, circular orbit, equal-mass case just discussed $\mathcal{R} = 350 \text{ km}/206 \text{ km} \sim 1.7$. The fact that the Newtonian/Kepler evolution of the orbit breaks down when the separation is about the order of the black hole sizes (compactness ratio \mathcal{R} of order 1) is further evidence that the objects were black holes.

IV. REVISITING THE ASSUMPTIONS

In Sec. III we demonstrated that the coalescing objects are black holes under the assumptions of a circular orbit, equal masses, and no spin. It is not possible, working at the level of approximation that we are using here, to directly constrain these parameters of the system (although more advanced techniques are able to constrain them, see Ref. 2). However, it is possible to examine how these assumptions affect our conclusions and in this section we

show that their consideration does not significantly change the outcome.

A. Eccentricity

First, for general non-circular orbits (eccentric) orbits, Kepler's third law (Eq. 9) holds if R is no longer interpreted as the orbital separation but rather as the semi-major axis. As the instantaneous orbital separation r_{sep} is bounded from above by R , we see that the compactness bound imposed by eccentric orbits is even tighter (the compactness ratio \mathcal{R} is smaller). There is also a correction to the luminosity which depends on the eccentricity. However, this correction is significant only for highly eccentric orbits¹⁴. As the angular momentum that gravitational waves carry away causes the orbits to circularize faster than they shrink^{10,11}, this correction can be neglected.

B. Unequal masses

Next, it is easy to see that the compactness ratio \mathcal{R} also gets smaller with increasing mass-ratio, as that implies a higher total mass for the observed value of the Newtonian order chirp mass. To see this explicitly, we express the component masses and total mass in terms of M_c and q , as

$$\begin{aligned} m_1 &= M_c(1+q)^{1/5}q^{2/5}, \\ m_2 &= M_c(1+q)^{1/5}q^{-3/5}, \quad \text{and} \\ M &= m_1 + m_2 = M_c(1+q)^{6/5}q^{-3/5}. \end{aligned} \tag{10}$$

The compactness ratio \mathcal{R} is the ratio of the orbital separation R to the sum of the Schwarzschild radii of the two component masses, $r_{\text{Schwarz}}(M) = r_{\text{Schwarz}}(m_1) + r_{\text{Schwarz}}(m_2)$, giving

$$\mathcal{R} = \frac{R}{r_{\text{Schwarz}}(M)} = \frac{c^2}{2(\omega_{\text{Kep}}|_{\max} GM)^{2/3}} = \frac{c^2}{2(\pi f_{\text{GW}}|_{\max} GM_c)^{2/3}} \frac{q^{2/5}}{(1+q)^{4/5}} \approx \frac{3.0 q^{2/5}}{(1+q)^{4/5}}. \tag{11}$$

This quantity is plotted in Fig. 5, which clearly shows that for mass ratios $q > 1$ the compactness ratio *decreases*: the separation between the objects becomes smaller when measured in units of the sum of their Schwarzschild radii. Thus, for a given chirp mass and orbital frequency, a system composed of unequal masses is *more* compact than one composed of equal masses.

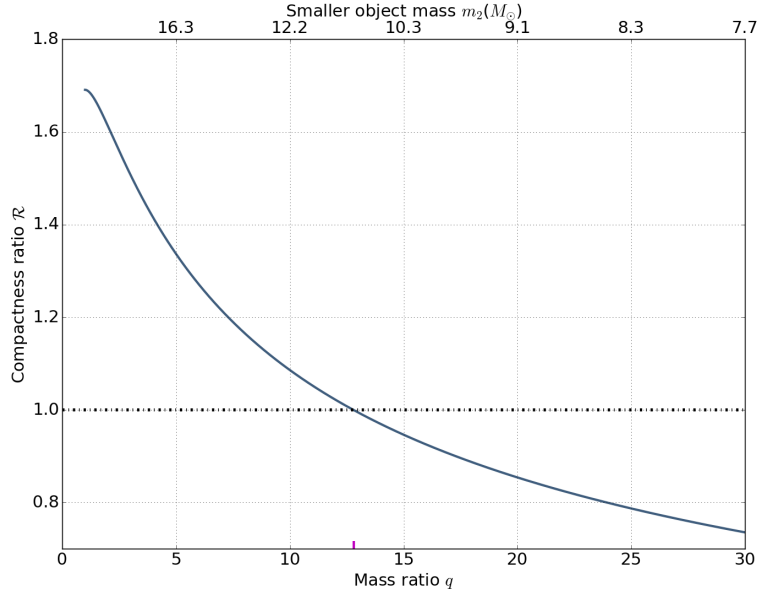


FIG. 5. The compactness ratio of the separation between the two objects to their Schwarzschild radii as a function of mass ratio. As shown in Eq. 11 the compactness ratio decreases as the mass ratio increases. So the argument given in Sec. III also applies for unequal masses. We note that beyond mass ratio of $q \sim 13$ the system becomes more compact than the sum their Schwarzschild radii.

One can also place an *upper* limit on the mass ratio q , thus a lower bound on the smaller mass m_2 , based purely on the data. This bound arises from minimal compactness: we see from the compactness ratio plot in Fig. 5 that beyond the mass ratio of $q \sim 13$ the system becomes so compact that it will be within the Schwarzschild radii of the combined mass of the two bodies. This gives us a limit for the mass of the smaller object $m_2 \geq 11 M_\odot$. As this is 3–4 times more massive than the neutron star limit, both bodies are expected to be black holes .

C. Spins

The third assumption we relax concerns the spins of the objects. The smallest radius a non-spinning object could have without being a black hole is its Schwarzschild radius. Allowing the objects to spin pushes the limit down by a factor of two, to the radius of an extremal Kerr black hole, $r_{EK}(m) = \frac{1}{2}r_{\text{Schwarz}}(m) = Gm/c^2$. As this is linear in the mass, and summing radii linearly we obtain a lower limit on the Newtonian separation of two

adjacent non-black hole bodies of total mass M is

$$r_{\text{EK}}(m_1) + r_{\text{EK}}(m_2) = \frac{1}{2}r_{\text{Schwarz}}(M) = \frac{GM}{c^2} \approx 1.5 \left(\frac{M}{M_\odot} \right) \text{ km.} \quad (12)$$

The compactness ratio can also be defined in relation to r_{EK} rather than r_{Schwarz} , which is at most a factor of two larger than for non-spinning objects.

We may thus constrain the orbital compactness ratio (now accounting for eccentricity, mass inequality and spin) by

$$\begin{aligned} \mathcal{R} &= \frac{r_{\text{sep}}(M)}{r_{\text{EK}}(M)} \leq \frac{R(M)}{r_{\text{EK}}(M)} = \frac{c^2}{(GM\omega_{\text{Kep}})^{2/3}} \\ &\leq \frac{c^2}{(2^{6/5}GM_c\omega_{\text{Kep}})^{2/3}} = \frac{c^2}{(2^{6/5}\pi GM_c f_{\text{GW}}|_{\max})^{2/3}} \simeq 3.4, \end{aligned} \quad (13)$$

where in the last step we used $M_c = 30 M_\odot$ and $f_{\text{GW}}|_{\max} = 150 \text{ Hz}$. This constrains the constituents to under 3.4 (1.7) times their extremal Kerr (Schwarzschild) radii, making them highly compact. The compact arrangement is shown in Fig. 4.

We can also derive an upper limit on the value of the mass ratio q , from the constraint that the compactness ratio must be larger than unity. This is because, for a fixed value of the chirp mass M_c and a fixed value of $f_{\text{GW}}|_{\max}$, the compactness ratio \mathcal{R} decreases as the mass ratio q increases. Thus, the constraint $\mathcal{R} \geq 1$, puts a limit on the maximal possible q and thus on the maximum total mass M_{\max} ,

$$\left(\frac{M_{\max}}{M_c} \right) \simeq 3.4^{3/2} \times 2^{6/5} \simeq 14.4, \quad (14)$$

which for GW150914 implies $M_{\max} \simeq 432 M_\odot$ (and $q \simeq 83$). This again forces the smaller mass to be at least $5 M_\odot$ - significantly above the neutron star mass limit.

The conclusion is the same as in the equal-mass or non-spinning case: both objects must have been black holes.

D. Newtonian dynamics

At this point we may also examine the applicability of Newtonian dynamics. The dynamics will diverge from the Newtonian approximation when the velocities approach the speed of light or when the gravitational energy becomes large compared to the rest energy. For a binary system these two limits coincide and may be quantified by the post-Newtonian

(PN) parameter $x \sim (v/c)^2 \sim GM/(c^2 r_{\text{sep}})$. Noticing that this expression includes the Schwarzschild radius, the dimensionless PN parameter can be immediately recast in terms of the compactness ratio, $x \sim 2/\mathcal{R}$. As Newtonian dynamics holds when x is small, it is seen that the Newtonian approximation is valid down to compactness \mathcal{R} of order of a few. In other words, in order to argue against the assumptions used to show that the orbit is compact, one would have to stipulate that the orbit is in fact compact.

Similarly, one could argue that using the coordinate R for the comparison of the Keplerian separation to the corresponding compact object radii is not entirely general. Here too, the errors in using these coordinates are non-negligible only very close to the horizon of a black hole, so again this argument does not refute our conclusions.

E. Is the chirp mass well measured – constraints on the individual masses

As we are analyzing the final cycles before merger, having accepted that they were compact, one might still ponder whether Eq. 7 correctly describes the chirp mass in the non-Newtonian regime. In fact for the last orbits, it does not: while in Newtonian dynamics stable circular orbits may exist all the way down to merger, in general relativity the last orbits for compact objects (at least when one of the objects is much larger) become plunges. The changes in orbital separation and orbital frequency in the final revolutions are thus not driven by the gravitational wave emission given by Eq. 7. This is why we used $f_{\text{GW}}|_{\text{max}}$ of the early visible cycles, rather than $f_{\text{GW}}|_{\text{fin}}$.

We shall now constrain the individual masses based on $f_{\text{GW}}|_{\text{fin}}$, for which we do not need the Newtonian approximation at the late stage. No neutron stars have been observed above $3 M_{\odot}$; we shall rely on an even more conservative neutron star mass upper bound at $4.76 M_{\odot}$, a value chosen because given M_c from the early visible cycles, in order for the smaller mass m_2 to be below this threshold, m_1 must be at least $476 M_{\odot}$, which implies $q \geq 100$. Is such a high q possible with the data that we have? Such a high mass ratio suggests a treatment of the system as an extremal mass ratio (EMR), where the smaller mass approximately follows a geodesic orbit around the larger mass ($m_1 \sim M$). The frequencies of test-particle orbits (hence waveforms) around an object scale with the inverse of its mass, and also involve its dimensionless spin χ . The orbital frequency ω_{orb} as measured at infinity of a circular,

equatorial orbit at radius r (in Boyer-Lindquist coordinates) is given by¹⁵

$$\omega_{\text{orb}} = \frac{\sqrt{GM}}{r^{3/2} + \chi \left(\sqrt{GM}/c \right)^3} = \frac{c^3}{GM} \left(\chi + \left(\frac{r}{GM/c^2} \right)^{3/2} \right)^{-1} \quad (15)$$

For example, around a Schwarzschild black hole ($\chi = 0$) the quadrupole gravitational wave frequency at the innermost stable circular orbit (ISCO, which is at $r = 6GM/c^2$) is hence equal to $f_{\text{GW}} = 4.4(M_{\odot}/M)$ kHz, while for an extremal Kerr black hole ($\chi = 1$) the orbital frequency at innermost stable circular orbit ($r = GM/c^2$) is $\omega_{\text{orb}} = c^3/2GM$, and the quadrupole gravitational frequency is $f_{\text{GW}} = c^3/2\pi GM = 32(M_{\odot}/M)$ kHz. For a gravitational wave from the final plunge orbits, the highest expected frequency is approximately the frequency from the light ring (LR), as nothing physical is expected to rotate faster than light. The light ring is at

$$r_{\text{LR}} = \frac{2GM}{c^2} \left(1 + \cos \left(\frac{2}{3} \cos^{-1}(-\chi) \right) \right). \quad (16)$$

This radius is $3GM/c^2$ for a Schwarzschild black hole , while for a spinning Kerr black hole , as the spin χ increases the light ring radius decreases. For an extremal Kerr black hole it coincides with the innermost stable circular orbit , at GM/c^2 . The maximal gravitational wave frequency for a plunge into m_1 is then 67 Hz.

Because we see gravitational wave emission from orbital motion at frequencies much higher than this maximal value, with or without spin, such a system is ruled out. Hence even the lighter of the masses is above $4.76 > 3 M_{\odot}$, beyond the maximum observed mass of neutron stars.

F. Possible redshift of the masses – a constraint from the luminosity

Gravitational waves are stretched by the expansion of the Universe as they travel across it. This increases the wavelength and decreases the frequency of the waves observed on Earth relative to their values when emitted, similar to the redshift effect of photons from distant objects. The impact of this on the gravitational wave phasing is similar to a scaling of the masses as measured on Earth; dimensional analysis of Eq. 7 shows that the source frame masses are smaller by $(1+z)$ relative to the detector frame, where z is the redshift. As direct inspection of the detector data yields mass values of the red-shifted waves, it could

be argued that the source frame values are actually significantly different from their values at the source. In order to estimate the impact of this effect, we now relate the amplitude and luminosity of the gravitational wave from the merger to the strain and flux measured at the detector, in order to estimate the distance to the source and hence the red-shift effect.

As the two objects merge and create the disturbance carried as gravitational waves , the strain can be at most $h \sim 1$, at a radius of the order of the Schwarzschild radius of the system $R \sim 100$ km. The measured strain peaks at $h|_{\max} \sim 10^{-21}$, and as the amplitude decreases as $h \sim R/d_L$ (with d_L the luminosity distance), we find

$$d_L \leq 10^{21} \times 100 \text{ km} \sim 3 \text{ Gpc}. \quad (17)$$

We can have an even better estimate based on the luminosity. The gravitational wave luminosity from a binary inspiral reaches an almost universal peak, which can be used to determine the source system's distance. First, we take the Planck Luminosity as a limit on the luminosity of any physical system¹⁶, using the following argument¹⁷: assume an energy Mc^2 emitted at light speed from a sphere of radius $R \implies$ luminosity Mc^3/R . Since R cannot be smaller than $R = GM/c^2$ (extremal Kerr limit), any luminosity is at most

$$L_{\text{Planck}} = Mc^3 / (GM/c^2) = c^5/G = 3.6 \times 10^{52} \text{ W} \quad (18)$$

For a binary inspiral, a naive dimensional analysis of the quadrupole formula would give a luminosity $L \sim \frac{G}{c^5} M^2 r^4 \omega^6$, with $\omega \sim c/r$ and $r \sim GM/c^2$, and $M\omega \sim c^3/G$ for the final tight orbit. Together this gives $L \sim c^5/G = L_{\text{Planck}}$. However, a closer look (Eq. A3) shows the prefactor could be approximated by that of a similar-mass system $(\frac{32}{5} (\frac{\mu}{M})^2 \sim 0.4)$. Also, analysis of a small object falling unto a Schwarzschild black hole suggests $M \sim \frac{1}{6} c^2 r_{\text{ISCO}}/G$ and $\omega r \sim 0.5c$. Taken together with the correct exponents, L acquires a factor $0.4 \times 6^{-2} \times 0.5^6 \sim 0.2 \times 10^{-3}$.

Using Eq. 5 we relate the luminosity of gravitational waves to their strain h at luminosity distance d_L ,

$$L \sim \frac{c^3 d_L^2}{4G} |\dot{h}|^2 \sim \frac{c^5}{4G} \left(\frac{\omega_{\text{GW}} d_L h|_{\max}}{c} \right)^2. \quad (19)$$

Thus we have $0.2 \times 10^{-3} \sim \frac{1}{4} (\omega_{\text{GW}} d_L h|_{\max}/c)^2$, and we can estimate the distance from the change of the measured strain in time over the cycle at peak amplitude, as

$$d_L \sim 45 \text{ Gpc} \left(\frac{\text{Hz}}{f_{\text{GW}}|_{\max}} \right) \left(\frac{10^{-21}}{h|_{\max}} \right), \quad (20)$$

which for GW150914 gives $d_L \sim 300$ Mpc. For a different distance-luminosity calculation based only on the strain data, see Ref. 18.

This distance corresponds to a redshift of $z \leq 0.1$, thus none of the arguments nor conclusions given above change beyond the 10% level.

V. CONCLUSIONS

A lot of physics and physical insight can be obtained by applying simple arguments to the observed strain data of GW150914. These are enough to show the system that produced the gravitational wave had been a pair of inspiraling black holes that approached very closely before merging. The system is seen to settle down, most likely to a single black hole. Simple arguments can also give us information about the system's distance and basic properties (for a related phenomenological approach see Ref. 19). More advanced analyses can give us even more information, and we encourage the reader to read how such analyses and models have been used for estimating the parameters of the system², for testing and constraining the validity of General Relativity in the highly relativistic, dynamic regime³ and for the study of astrophysics based on this event⁴. We hope this paper will serve as an invitation to the field, at the beginning of the era of gravitational wave observations.

ACKNOWLEDGMENTS

Appendix A: Calculation of gravitational radiation from a binary system

Here we outline the calculation of the energy a binary system emits in gravitational waves, and its effect on the system.

First we calculate the quadrupole moment Q_{ij} of the system's mass distribution. We use a Cartesian coordinate system $\mathbf{x} = (x_1, x_2, x_3) = (x, y, z)$ whose origin is the center-of-mass, with r the radial distance from the origin. $\delta_{ij} = \text{diag}(1, 1, 1)$ is the Kronecker δ and $\rho(\mathbf{x})$ denotes the mass density. Then

$$Q_{ij} = \int d^3x \rho(\mathbf{x}) (x_i x_j - \frac{1}{3} r^2 \delta_{ij}) = \sum_{A \in \{1,2\}} m_A \begin{pmatrix} \frac{2}{3} x_A^2 - \frac{1}{3} y_A^2 & x_A y_A & 0 \\ x_A y_A & \frac{2}{3} y_A^2 - \frac{1}{3} x_A^2 & 0 \\ 0 & 0 & -\frac{1}{3} r_A^2 \end{pmatrix}, \quad (\text{A1})$$

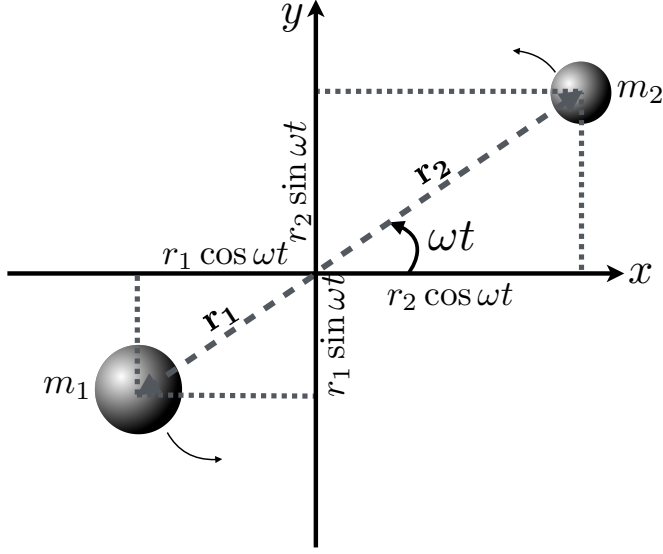


FIG. 6. A two-body system, m_1 and m_2 orbiting in the xy -plane around their center of mass.

where the second equality holds for a system of two bodies $A \in \{1, 2\}$ in the xy -plane. In the simple case of a circular orbit at separation $r = r_1 + r_2$ and frequency $f = \frac{\omega}{2\pi}$, a little trigonometry gives for each object (see Fig. 6)

$$Q_{ij}^A(t) = \frac{m_A r_A^2}{2} I_{ij}, \quad (\text{A2})$$

where $I_{xx} = \cos(2\omega t) + \frac{1}{3}$, $I_{yy} = \frac{1}{3} - \cos(2\omega t)$, $I_{xy} = I_{yx} = \sin(2\omega t)$ and $I_{zz} = -\frac{2}{3}$. Combining we find $Q_{ij}(t) = \frac{1}{2}\mu r^2 I_{ij}$, where we have used the standard reduced mass $\mu = m_1 m_2 / M$, and the gravitational wave luminosity from Eq. 5 is

$$\frac{d}{dt} E_{\text{GW}} = \frac{32}{5} \frac{G}{c^5} \mu^2 r^4 \omega^6. \quad (\text{A3})$$

This energy loss drains the orbital energy $E_{\text{orb}} = -\frac{GM\mu}{2r}$, thus $\frac{d}{dt} E_{\text{orb}} = \frac{GM\mu}{2r^2} \dot{r} = -\frac{d}{dt} E_{\text{GW}}$.

Using Kepler's third law $r^3 = GM/\omega^2$ and its derivative $\dot{r} = -\frac{2}{3}r\dot{\omega}/\omega$ we can substitute for all the r 's and obtain

$$\dot{\omega}^3 = \left(\frac{96}{5}\right)^3 \frac{\omega^{11}}{c^{15}} G^5 \mu^3 M^2 = \left(\frac{96}{5}\right)^3 \frac{\omega^{11}}{c^{15}} (GM_c)^5, \quad (\text{A4})$$

having given the symbol M_c to the mass quantity $M_c = (\mu^3 M^2)^{1/5}$.

We can see that Eq. A4 describes the evolution of the system as an inspiral: the orbital frequency goes up (“chirps”), while by Kepler's Law the orbital separation shrinks.

Appendix B: Possibilities for massive, compact objects

We are considering astrophysical objects on the mass scale of $m \sim 35 M_{\odot}$, which are constrained to fit into a radius R such that the compactness ratio obeys $\mathcal{R} = \frac{c^2 R}{G m} \lesssim 3.4$. This produces a scale for their Newtonian density,

$$\rho \geq \frac{m}{(4\pi/3)R^3} = 3 \times 10^{15} \left(\frac{3.4}{\mathcal{R}}\right)^3 \left(\frac{35 M_{\odot}}{m}\right)^2 \frac{\text{kg}}{\text{m}^3}, \quad (\text{B1})$$

where equality is attained for a uniform object. This is a factor of 10^6 more dense than white dwarfs, so we can rule out objects supported by electron degeneracy pressure, as well as any main-sequence star, which are sparser. While this density is a factor of $\sim 10^2$ less dense than neutron stars, these bodies exceed the maximum neutron star mass by an order of magnitude, as the neutron star limit is $\sim 3M_{\odot}$ ($3.2 M_{\odot}$ in Refs. 20 and 21, $2.9 M_{\odot}$ in Ref. 22). A more careful analysis of the frequency change, including tidal distortions, would have undoubtedly required the bodies to be even more compact in order to reach the final orbital frequency. This would push these massive bodies even closer to neutron-star density, thus constraining the equation of state into an even narrower corner. Thus, although theoretically a compactness ratio as low as $\mathcal{R} = 4/3$ is permitted for uniform objects²³, we can conclude that the data do show that if any of these objects were material bodies, they would need to occupy an extreme, narrow and heretofore unexplored and unobserved niche in the stellar continuum. The likeliest objects of such masses and compactness are black holes.

Appendix C: Post inspiral phase: what we can conclude about the ringdown and the final object?

We have argued, using basic physics and scaling arguments, that the directly observable properties of the signal waveform for gravitational wave frequencies $f_{\text{GW}} < 150$ Hz shows that the source had been two black holes, which approached so closely that they subsequently merged. We now discuss the properties of the signal waveform at higher frequencies, and argue that this also lends support to this interpretation.

The data in Figures 1 and 2 show that after the peak gravitational wave amplitude is reached, the signal makes a few more complete cycles, and continues to rise in frequency

until reaching about 250 Hz, while dropping sharply in amplitude. The frequency seems to level off just as the signal amplitude becomes hard to distinguish clearly.

Is this consistent with a merger remnant black hole? Immediately after being formed in a merger, a black hole horizon is very distorted. It proceeds to “lose its hair” and settle down to a final state of a Kerr black hole, uniquely defined²⁴ by its mass M and spin parameter χ . Long enough into this ringdown stage, the remaining perturbations should linearize, and the emitted gravitational wave should thus have characteristic quasi-normal-modes (QNMs). The set of QNMs is enumerated by various discrete indices, and their frequencies and damping times are determined by M and χ . Each such set would have a leading (least-damped) mode – and so finding a ringdown of several cycles with a fixed frequency would be strong evidence that a single final remnant was formed. We do clearly see the gravitational wave stabilizing in frequency (at around 250 Hz) about two cycles after the peak, and dying out in amplitude – does the end of the observed waveform contain evidence of an exponentially-damped sinusoid of fixed frequency? Were such a mode found, analyzing its frequency and damping time, in conjunction with a model for black hole perturbations, could give an independent estimate of the mass and spin²⁵.

1. Mode Analysis

The ringing of a Kerr black hole can be thought of as related to a distortion of space-time traveling on light ring orbit outside the black hole horizon (See Ref. 26 and references therein, and Eqs. (15, 16)); the expected frequency for a quadrupolar mode ($\ell = m = 2$) will thus be given as a dimensionless complex number

$$\frac{G}{c^3} M \omega_{\text{GW}} = x + iy. \quad (\text{C1})$$

The ringdown amplitude and damping times are then found from

$$e^{i\omega_{\text{GW}}t} = e^{i(c^3x/GM)t} e^{-(c^3y/GM)t} = e^{2\pi i f_{\text{GW}}|_{\text{ringdown}} t} e^{-t/\tau_{\text{damp}}}, \quad (\text{C2})$$

to be $f_{\text{GW}}|_{\text{ringdown}} = c^3x/(2\pi GM)$ and $\tau_{\text{damp}} = GM/c^3y$.

The exact values of x and y can be found as when analyzing the normal modes of a resonant cavity: one uses separation of variables to solve the field equations, and then enforcing the boundary conditions results in a discrete set of complex eigenfrequencies²⁶.

However, limiting values on x , $x \in (\sim 0.3, 1]$, are derived immediately from Eqs. (15, 16), with a factor of 2 between orbital and gravitational wave frequencies. The final gravitational wave frequency is thus determined by the mass (up to the order-of-unity factor x , which embodies the spin). We have in fact already used this to show how our high attained frequency constrains the total mass and the compactness of the objects (objects of larger radius would have distortion bulges orbiting much farther than the light ring, mandating much lower frequencies). As for the parameter y determining the damping time, numerical tabulations of the QNMs²⁶ show that

$$f_{\text{GW}}|_{\text{ringdown}} \tau_{\text{damp}} = \frac{x}{2\pi y} \sim 1 \quad \text{for a broad range of spins and mode numbers .} \quad (\text{C3})$$

This shows that we do expect the ringdown to have a damping time roughly equal to the period of oscillation. This is exactly what is seen in the waveform, and is the reason the signal amplitude drops so low by the time the remnant rings at the final frequency.

While it is beyond the scope of this paper to calculate the exact QNMs for black holes of different spins, or to find the final spin of a general black hole merger, it is worth mentioning that for a wide range of spins for similar-mass binaries, the final spin is expected to be about $\chi \sim 0.7$, for which eq. (15, 16) estimate that $\text{Re}[\frac{G}{c^3} M \omega_{\text{GW}}] \sim 0.55$.

The exact value can be found using Table II in Ref. 26, where the leading harmonic ($\ell = 2, m = 2, n = 0$) for a black hole with a spin $\chi = 0.7$ has $\frac{G}{c^3} M \omega_{\text{GW}} = 0.5326 + 0.0808i$, giving a ringdown frequency

$$f_{\text{GW}}|_{\text{ringdown}} \approx 245 \text{ Hz} \left(\frac{70 \text{ M}_\odot}{M} \right) , \quad (\text{C4})$$

and a damping time

$$\tau_{\text{damp}} = 0.00427 \text{ seconds} \left(\frac{M}{70 \text{ M}_\odot} \right) \sim \frac{1}{f_{\text{GW}}|_{\text{ringdown}}} . \quad (\text{C5})$$

In other words, the signal in the data is fully consistent¹⁸ with the final object being a Kerr black hole with a dimensionless spin parameter $\chi \sim 0.7$ and a mass $M \sim 70 \text{ M}_\odot$. This interpretation of the late part of the signal is also consistent with numerical simulations²⁷. Full numerical simulations from the peak and onward, where the signal amplitude is considerably

higher, also show consistency with the formation of a Kerr black hole remnant^{2,3}.

- ¹ B. P. Abbott *et al.* (LIGO Scientific, Virgo), *Phys. Rev. Lett.* **116**, 061102 (2016), arXiv:1602.03837 [gr-qc].
- ² B. P. Abbott *et al.* (LIGO Scientific, Virgo), (2016), arXiv:1602.03840 [gr-qc].
- ³ B. P. Abbott *et al.* (LIGO Scientific, Virgo), (2016), arXiv:1602.03841 [gr-qc].
- ⁴ B. P. Abbott *et al.* (LIGO Scientific, Virgo), *Astrophys. J.* **818**, L22 (2016), arXiv:1602.03846 [astro-ph.HE].
- ⁵ K. S. Thorne, in *Magic Without Magic*, edited by J. R. Klauder (Benjamin Press, San Francisco, 1972) pp. 231–258.
- ⁶ The advanced LIGO detectors use laser interferometry to measure the strain caused by passing gravitational waves. It is not our intention here to describe how the detectors work; for details see Ref. 1 and its references.
- ⁷ When the signal amplitude is lower and the noise makes the signal’s sign transitions difficult to pinpoint, we averaged the positions of the (odd number of) adjacent zero-crossings.
- ⁸ L. D. Landau and E. M. Lifshitz, *The Classical Theory of Fields*, 4th ed., Vol. 2 (Elsevier, Oxford, 1975) pp. 356–357.
- ⁹ A. Einstein, Sitzungsberichte der Königlich Preußischen Akademie der Wissenschaften (Berlin), Seite 154-167 (1918).
- ¹⁰ P. C. Peters and J. Mathews, *Phys. Rev.* **131**, 435 (1963).
- ¹¹ P. C. Peters, *Gravitational Radiation and the Motion of Two Point Masses*, Ph.D. thesis, Caltech (1964).
- ¹² L. Blanchet, T. Damour, B. R. Iyer, C. M. Will, and A. G. Wiseman, *Phys. Rev. Lett.* **74**, 3515 (1995).
- ¹³ One could argue that identification of a rigid reference frame for measuring distances between points is not unique in Relativity. However, this complication arises only with large gravitational potentials, while in the Keplerian regime (of low compactness and low potentials) the system’s center-of-mass rest-frame can be used. Therefore if the system is claimed to be non-compact, the Keplerian argument should hold, and constrain the distances to be compact (see Sec. IV D). We conclude the assumption of non-compactness is refuted.

- ¹⁴ Eccentricity increases the luminosity^{10,11} by a factor $\ell(e) = (1 - e^2)^{-7/2} (1 + \frac{73}{24}e^2 + \frac{37}{96}e^4) \geq 1$, thus reducing the chirp mass to $M_c(e) = \ell^{-3/5}(e) \cdot M_c(e=0)$. Together with the factor between the periastron and the semi-major axis, $\mathcal{R}(e) = (1 - e)\ell^{2/5}(e) \cdot \mathcal{R}(e=0)$. Hence for the compactness ratio to increase the eccentricity must be $e \gtrsim 0.6$, and for a factor of 2, $e \gtrsim 0.9$.
- ¹⁵ J. M. Bardeen, W. H. Press, and S. A. Teukolsky, *Astrophys. J.* **178**, 347 (1972).
- ¹⁶ F. Dyson, in *Interstellar Communication*, edited by A. G. W. Cameron (Benjamin Press, New York, 1963) Chap. 12.
- ¹⁷ C. J. Hogan, (1999), arXiv:astro-ph/9912110 [astro-ph].
- ¹⁸ L. M. Burko, (2016), arXiv:1602.04666 [physics.ed-ph].
- ¹⁹ J. F. Rodriguez, J. A. Rueda, and R. Ruffini, (2016), arXiv:1605.04767 [gr-qc].
- ²⁰ C. E. Rhoades, Jr. and R. Ruffini, *Phys. Rev. Lett.* **32**, 324 (1974).
- ²¹ M. Hannam, D. A. Brown, S. Fairhurst, C. L. Fryer, and I. W. Harry, *Astrophys. J.* **766**, L14 (2013), arXiv:1301.5616 [gr-qc].
- ²² V. Kalogera and G. Baym, *Astrophys. J.* **470**, L61 (1996), arXiv:astro-ph/9608059 [astro-ph].
- ²³ J. M. Lattimer, Annual Review of Nuclear and Particle Science **62**, 485 (2012), <http://dx.doi.org/10.1146/annurev-nucl-102711-095018>.
- ²⁴ B. Carter, *Phys. Rev. Lett.* **26**, 331 (1971).
- ²⁵ W. H. Press and S. A. Teukolsky, *Astrophys. J.* **185**, 649 (1973).
- ²⁶ E. Berti, V. Cardoso, and C. M. Will, *Phys. Rev. D* **73**, 064030 (2006), arXiv:gr-qc/0512160 [gr-qc].
- ²⁷ I. Kamaretsos, M. Hannam, S. Husa, and B. S. Sathyaprakash, *Phys. Rev. D* **85**, 024018 (2012).